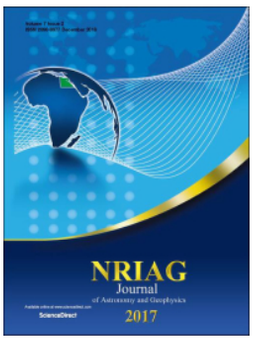

NRIAG Journal of Astronomy and Geophysics

ISSN: (Print) (Online) Journal homepage: https://www.tandfonline.com/loi/tjag20

Electrical resistivity imaging and multichannel analysis of surface waves for mapping the subsurface of a Wetland Area of Lagos, Nigeria

C.C. Uwaezuoke, K.S. Ishola & E. A. Ayolabi

To cite this article: C.C. Uwaezuoke, K.S. Ishola & E. A. Ayolabi (2021) Electrical resistivity imaging and multichannel analysis of surface waves for mapping the subsurface of a Wetland Area of Lagos, Nigeria, NRIAG Journal of Astronomy and Geophysics, 10:1, 300-319, DOI: 10.1080/20909977.2021.1927427

To link to this article: https://doi.org/10.1080/20909977.2021.1927427

Published online: 24 May 2021.

NRIAG JOURNAL OF ASTRONOMY AND GEOPHYSICS
2021, VOL. 10, NO. 1, 300–319
https://doi.org/10.1080/20909977.2021.1927427

Electrical resistivity imaging and multichannel analysis of surface waves for mapping the subsurface of a Wetland Area of Lagos, Nigeria

C.C. Uwaezuoke[a], K.S. Ishola[a] and E. A. Ayolabi[a,b]

[a]Dept. Of Geosciences, University of Lagos, Akoka, Nigeria; [b]Dept. Of Geosciences, Mountain Top University, Abeokuta, Nigeria

ABSTRACT

Electrical resistivity imaging (ERI) and Multichannel Analysis of Surface Waves (MASW) surveys were carried out over a reclaimed wetland area of University of Lagos, Nigeria. The main purpose of the geophysical surveys was to characterise the site for better understanding of the subsurface conditions before building construction is carried out. For this purpose, seven traverses were established for electrical resistivity and surface waves measurements. The PASI resistivity metre was used for the ERI surveys with minimum electrode spacing of 5 m using the Wenner array. The MASW measurements were carried out using Terraloc seismograph with 24 channel 4.5 Hz vertical component geophones. The results of the ERI surveys show that the subsurface strata are composed of peat/organic materials with resistivity values of (0.7– 3) Ω-m, silty clay having resistivity values of (5– 50) Ω-m and sandy clay sediments of resistivity between (51– 105) Ω-m, all were mapped at different depths. Also, the shear wave velocity models from MASW measurements show that three zones were clearly mapped. These zones are the low shear strength strata of peat/organic materials with Vs between (25– 70) m/s, silty clay with Vs ranges between (70– 120) m/s and sandy clay of Vs ranging from (120– 150) m/s. The combined approach has helped to better define the interface between layers, their thicknesses and consistency of each stratum. Thus, moderate to very strong correlations between the measured resistivity and velocity and the boreholes drilled were achieved. The regression models obtained compared reasonably well for all the traverses. The engineering implication of the geological units mapped is that the site is characterised with weak/incompetent materials not suitable for hosting the foundation of especially massive engineering structures. Hence, deep foundation through pilling to the competent layer is to be giving consideration or soils improvement techniques can be employed for the stabilisation of the soils.

ARTICLE HISTORY
Received 3 June 2019
Revised 1 May 2021
Accepted 4 May 2021

KEYWORDS
Electrical resistivity; Shear strength; Wenner Array; Geophone; Foundation; Borehole

1. INTRODUCTION

The need for shelters in a densely populated area like Lagos Metropolis southwestern, Nigeria has led to a continued increase in structural development of massive engineering structures particularly in the wetlands. Wetlands are portions of the land that are saturated with water and play vital roles in the sustenance of both Earth's surface and groundwater resources (Yan and Ming-Xiang 2001; Ajibola et al. 2012; Desta et al. 2012). Habitats such as peatlands, marshes, floodplains, coastal salt marshes, and mangroves are examples of wetlands. More specifically, wetlands consist of permanent or seasonal saturated soil types, and distinct vegetation combined to supports the ecosystem. There is no gainsaying that wetlands regions are of great values to both for habitations and the services they provide (Maltby 2009).

In recent times, Lagos, the biggest city in Nigeria has continued to witness spate of building collapse, tilting or cracks in buildings caused by differential settlement, particularly in the wetland areas. Sequel to this unfortunate incidence, many reasons has been suggested as the possible causes of building collapse/failure in buildings/engineering structures (Oyedele and Olorode 2010; Ayolabi et al. 2012; Adiat et al. 2017; Adeoti et al. 2018). Among these gamut of reasons are soil liquefaction resulting in severe damages (Bakir et al. 2002; Rezaeian and Gruen 2007; Tokimatsu et al. 2012), the manner in which buildings are utilised (Olusola and AKINTAYO 2009), construction practices and maintenance of structures (Ayedun et al. 2012; Olagunju et al. 2013; Chendo and Obi 2015; Usmen and Vilnitis 2015) and presence of smectite in the soils (Mckinley et al. 2003). Field and laboratory tests, however, have shown that building failures are not only due to usage, inadequate supervision, use of substandard building materials, non-compliance to specifications but also due to inadequacy in understanding the soil conditions regarding to characteristics and physical behaviour of the soils on which the buildings are built.

CONTACT K.S. Ishola saidisho@yahoo.co.uk; kishola@unilag.edu.ng

This article has been republished with minor changes. These changes do not impact the academic content of the article.

In the context of science, geoscientists and other soil practitioners have identified lack of adequate knowledge of the subsurface conditions as a major factor responsible for the collapse in structures. In addition, geological factors such as near surface geologic sequence, existing geological structures such as fractures/faults, boulders, voids, sinkholes, and the presence of weak/shear zones all constitute geohazards that can impair the stability of any engineering structure (Oyediran and Famakinwa 2015; Adiat et al. 2017).

Soil characterisation serves as pre-investigation exercise before building construction is carried out especially for superstructures. Soil characterisation using the traditional techniques of borehole drillings at specific locations is used to produce a model of soil layers as well as gathering high-vertical-resolution data on textural properties (Van Dam 2012). The Cone Penetrometer Tests (CPT) and Standard Penetrometer Tests (SPT) are examples of boring tests that are not enough to meet today's needs for site characterisation because they provide only point source information with respect to the subsurface stratigraphy. Also, these techniques are not only costly to scale up to the degree of spatial coverage needed for more detailed analysis of the soils but also being invasive making it impracticable to carry out repeated measurements necessary for an optimum characterisation of subsurface conditions.

Geophysical methods which are usually non-invasive have proven to be very vital tools for analysing and characterising the subsurface conditions for groundwater and engineering applications due to their large sampling rate (Giao et al. 2003; Papadopoulos et al. 2006; Soupios et al. 2007; Anderson et al. 2008; Popp et al. 2013). Moreso, the geophysical methods have been reported to enhance the reliability, speed, and reduction in cost of geotechnical investigations (Anderson et al. 2008; Arjwech and Everett 2015). The use of geophysical methods for stratigraphic mapping rely on a good contrast in the physical properties being measured making them necessary and adequate for picturing the subsurface.

The application of geophysical methods especially in soil investigations of the wetland areas is limited in literature especially the seismic surface waves method. Elsewhere, the wetland regions were investigated to clearly understand subsurface geology (Comas et al. 2004; Kettridge et al. 2008; Chambers et al. 2014). Mansoor and Slater (2007) used Electrical Resistivity Imaging (ERI) survey for the investigation of spatial and temporal variations of fluid conductivity in wetland soils. In another studies, (Ayolabi et al. 2012; Adeoti et al. 2018) used geophysical and geotechnical methods for the characterisation of subsurface geological units in wetland area of coastal plain of Lagos. A time-lapse geoelectrical imaging of wetland for hydrological processes was carried out (Uhlemann et al. 2016). Adegbola *et al.*, 2016 investigated the causes of road failure and land subsidence using Multichannel Analysis of Surface Waves (MASW) technique. A collection of published electrical resistivity and surface waves velocity values for different soils in wetland areas of Lagos is presented in Table 1.

Table 1. Published electrical resistivity and surface waves values for soils in wetland areas.

Soil/Material	Resistivity (Ωm)	Shear waves velocity (m/s)	Geophysical Method	Reference
Silty sandy clay	20– 50		2D ERI	Ayolabi et al. 2012
Peat/clay	2.4– 18			
Silty sand/ sandy clay	90– 190			
Clay	20– 30		2D ERI	Oyedele et al., 2015
Silty sand	< 160			
Soft clay/ very poor rock		60– 70	MASW	Adegbola et al., 2012
Soft clay/ poor rock		70– 80		
Firm clay/fair rock		80– 90		
Silty clay/fair rock		90– 100		
Peat/Organic clay		60– 90	MASW	Adegbola et al. 2016
Soft/loose soil		111– 140		
Peat/clay		40– 120	MASW	Adeoti et al. 2018
Loose fills/ soft clays		140– 240		
Sand sediments		503– 910		
Peat/clay	2– 5		1D VES	Adeoti et al. 2018
Clay	11– 16			
Sandy clay	61– 76			
Reclaimed soils	54– 155			
	1– 115		2D ERI	Adeoti et al. 2018
	1.6– 6.8			
	115– 900			

In this present study, an effort to better understanding the subsurface geology of the study area using the integration of ERI and MASW techniques was undertaken. This becomes necessary in order to achieve the following objectives: (i) delineate the subsurface soils into geologic sequence beneath the study area (ii) determine the geophysical properties of the soil and their suitability for the engineering structural development (iii) establish correlations between the measured physical parameters with a view to capturing the Geo-engineering information of the study area.

2. LOCATION, PHYSIOGRAPHY AND GEOLOGY OF THE STUDY AREA

The study area is a site (Figure 1) at Faculty of Science, University of Lagos, for the construction of a proposed

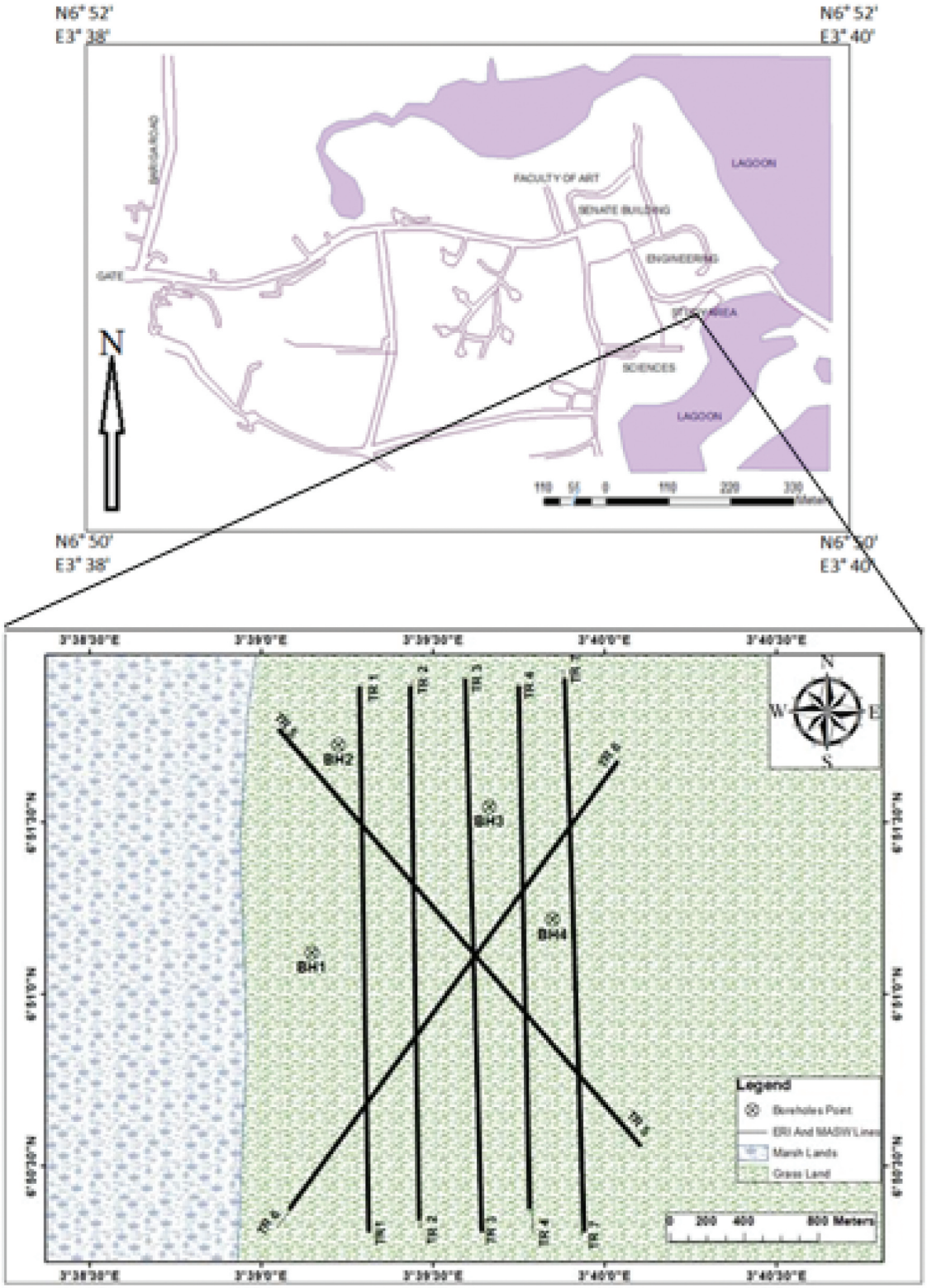

Figure1 Location map of the study area.

building for Institute of Maritime Studies. It lies between Latitudes N6° 50′ – N6° 52′ and Longitudes E3° 38′ – E3° 40′ with a total land area of 3577.28 km^2, out of which 22% is wetland (Sojobi et al. 2016). The site is a virgin land lying fallow for years with thick vegetation and marshy terrain. The naturally marshy near surface soil materials have invasively been de-compacted with a bulldozer and sand-filled in most part. Lagos State is bounded in the north by Ogun State, south by Atlantic Ocean and west by Benin Republic. The climatic condition is moderately hot and humid. There are two distinct seasons in the state, namely, the rainy season which lasts from March/April to October/November and the dry season which lasts for the rest of the year, October/

November till March/April (Nigeria Meteorological Agency (NIMET) 2007).

Lagos State is a zone of coastal Creeks and Lagoons (Pugh 1954) developed by barrier beaches associated with sand deposits (Hill and Webb 1958). The surface topography shows that the terrain is relatively flat. The surface geology is characterised by complex geologies of alternating sequences of clay and sand deposits (ranging from silt, clay, and fine to coarse grained sand) forming the Youngest stratigraphic called Benin Formation (Miocene to Recent) and Recent littoral alluvial deposits. The Benin Formation consists majorly of yellowish (Ferrugious) and white sand bodies (Jones and Hockey 1964).

The geomorphologic sub-units recognised in the area are Abeokuta, Imo group (Ewekoro and Akinbo), Oshoshun/Ilaro and Benin Formations (Adegoke et al. 2010). All these formations fall within the Dahomey Basin believed to be formed during the commencement of rifting, associated with the opening of the Gulf of Guinea in the early Cretaceous to late Jurassic (Adegoke et al. 2010). The Dahomey Basin extends from the south eastern Ghana through Togo and Benin Republic on the West side to the Okitipupa ridge/Benin Hinge line in the east side in the southern part of Nigeria (Adegoke et al. 2010). The geology of the basin had been improved through the availability of boreholes and recent road cuts. A simplified geological map of the study area is shown in Figure 2.

3. BASIC THEORY

3.1. Electrical resistivity studies

The electrical resistivity method is based on Ohm's Law (i.e. V = IR) and it is among the oldest geophysical survey techniques used for the investigation of the subsurface conditions. Electrical resistivity imaging (ERI) is becoming increasingly popular for investigating the near-surface conditions for a variety of applications. This includes but not limited to mapping saline water intrusion into fresh waters (Slater and Sandberg, 2000); assessment of peat properties (Kowalczyk et al. 2017); delineation of shallow-water wetlands (Mansoor and Slater 2007). Furthermore, ERI is used in several fields such as engineering, geological, archaeological, hydrogeological, and environmental studies due to the dependence of resistivity of subsurface heterogeneity on various parameters (Lapenna et al. 2003; Grandjean et al. 2006; Shemang and Molwalefhe 2009; Giang et al. 2013; Pacanowski et al. 2014; Amini and Ramazi 2016; Kowalczyk et al. 2017).

Electrical resistivity is a physical characteristic of a the subsurface that depends on factors such as porosity, grain cementation, compactness, water content, mineral composition and clay mineral (Dahlin and Zhou, 2006). A summary of the resistivity of some common geological materials is presented in Table 2. The resistivity of the ground is linked to various geological materials (Evrett 2013). The presence of any subsurface discontinuity could have a significant impact on a measured electrical resistivity thus a good electrical contrast or response may be obtained.

In subsurface mapping, the choice of a suitable electrode array configuration is another factor that determines the success of ERI (Ishola et al. 2014). Among the several electrode arrays commonly used in electrical resistivity survey are the standard arrays: the Wenner, Schlumberger, and dipole-dipole. Others

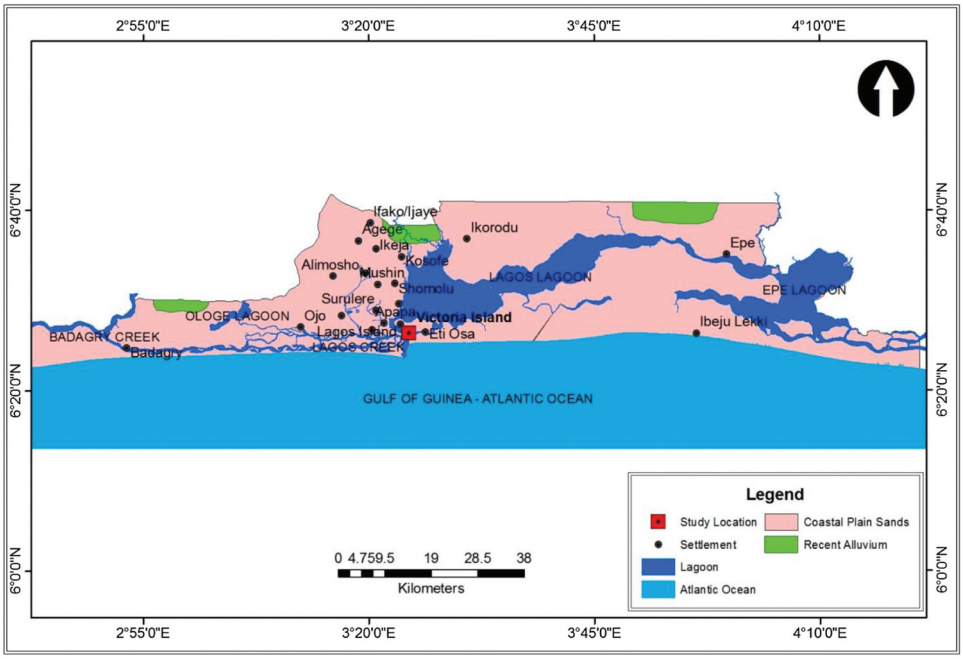

Figure 2. Geological map of Lagos State (culled from Olatinsu et al. 2018).

Table 2. Resistivity of common geological materials (modified after Evrett 2013).

Geomaterial	Resistivity (Ohm-m)
Salt water	0.1–1.0
Clay	1– 20
Silty clay	28– 80
Clayey silt	50– 120
Wet to moist sand	20– 200
Dry sand	1000– 4000
Shale	1– 500
Porous limestone	100 –1000
Gravel and sand	800– 10,000

are pole-dipole, pole – pole, and gradient arrays. The difference between these array types lies in the separation between the electrodes that provides variations or differences in the geometric factor for each array (Loke 2001). The conventional Wenner array is relatively sensitive to vertical changes in the subsurface resistivity but less sensitive to horizontal changes in the subsurface resistivity that is it is good at resolving vertical changes but relatively poor in detecting horizontal changes. The median depth of investigation (Ze) is defined as the depth obtained by integrating the sensitivity function with depth. Table 3 gives the Ze for the different arrangements of the Wenner array with the total length of survey equals to L. The depths are given as the ratio to the "a" spacing or the total length "L" of the array (Loke et al. 2003). The horizontal coverage for the Wenner array decreases with increasing electrode spacing (Gharibi and Bentley 2005). The sensitivity function which indicates the extent to which a change in the resistivity of a model will influence the potential measured by the array also decreases with depth for the Wenner array when compared to other array, say, dipole-dipole.

3.2. Seismic studies

In seismic surveying, seismic waves are generated by a controlled source, propagate through the subsurface and return to the surface after refraction and reflection at geological boundaries or travelling along free interface within the subsurface. Geophones arranged linearly along the surface are used to record the arrival times of the waves at different ranges from the source (Kearey et al. 2002). These travel times are converted into depth values and, hence, the distribution of subsurface geological interfaces may be mapped.

Table 3. The medium depth of investigation for the Wenner array (modified after Dobry et al. 1977).

Array type	Ze/a	Ze/L	Geometric Factor
Wenner Alpha (α)	0.519	0.173	6.2832
Wenner Beta (β)	0.416	0.139	18.850
Wenner Gamma (γ)	0.594	0.198	9.428

Seismic waves are divided into two categories; body waves and surface waves. Body waves are transmitted through the interior of the Earth and consist of compressional waves (P-waves/primary waves) and shear waves (S-waves/secondary waves). On the other-hand, surface waves the focus in this study, travel along the interface between two different media and are the results of interfering P-waves and/or S-waves (Xia et al. 2002).

A non-invasive seismic technique called the Multichannel Analysis of Surface Waves (MASW) was developed to determine the multilayered stratigraphy using the dispersive nature of surface waves. When a seismic signal is created on the ground surface, about 70% of the seismic energy travels in the form of surface waves. The MASW technique uses horizontally travelling Rayleigh-type surface waves to extract the near surface elastic properties of the subsurface (Park et al. 1999; . The MASW technique has been applied to seismic characterisation of pavements; detection of voids (Park et al. 1998), and sea bottom sediments characterisation . In Table 4 the shear wave velocity for different soil/rock types.

Dispersion is linked with waves travelling through a wider area with different frequency, wavelength, and phase velocity (Foti et al. 2003; Aggelis and Shiotani 2007). A situation where more than one phase velocities occurs at a given frequency is called multimodal dispersion. The slowest one is the fundamental mode and the next faster one is the first higher mode (Taipodia et al. 2015). Some of the inherent limitations of the refraction technique such as hidden layer, velocity inversions which result when a low velocity layer is overlain by a higher velocity layer, and the blind zone can be overcome using surface wave methods (Foti et al. 2003).

A well known limitation of the surface-wave technique is its trade-off between lateral resolution and depth of investigation. According to Bode *et al.* (2009), the spread length has to be short enough to achieve good lateral resolution if profiling is performed while long spreads are required to record wavelengths great enough to increase investigation depth.

The effective depth of penetration of a surface wave theoretically is commonly taken as one wavelength,

Table 4. Typical range of Shear waves velocity in soils and rocks (Nath 2008).

Soil/Rock	V_s (m/s)
Water	0
Clay/Silt	40– 250
Sand	80– 450
Weathered rock	250– 700
Bedrock	400– 700
Granite	1700– 3500
Fresh granite	1500– 3000

with most of the energy concentrated between the surface and depth of one-third of the maximum resolved wavelength (Park et al. 1999). Sequel to this, high frequencies (i.e. short wavelength) waves propagate at the velocity of the upper layer while lower frequencies (large wavelength) waves propagate at greater depth into the soil layers (Lai and Wilmanski 2005).

The phase difference as a function of frequency ($\Delta\emptyset(f))\Delta\emptyset(f)$) between two adjacent geophone is estimated using Eq.1.

$$\Delta\emptyset(f) = phase[G(f)F^*(f)]\Delta\emptyset(f) = phase[G(f)F^*(f)] \quad (1)$$

where:
G(f) and F(f) are the Fourier transforms of the time signals from the second and first receivers respectively and * represents the complex conjugate. The phase velocity at a given frequency (f) with spacing between adjacent geophones (Δx) is given by Eq. 2.

$$V_{phase}(f) = 2\pi f \frac{\Delta x}{\Delta\emptyset(f)} V_{phase}(f) = 2\pi f \frac{\Delta x}{\Delta\emptyset(f)} \quad (2)$$

Using the half-wavelength condition, Rix and Leipski (1991) proposed that the maximum depth of penetration (Z_{max}) for which Vs can be reasonably estimated to be equal to about half the longest wavelength (λ_{max}) measured and it is given in Eq. 3.

$$Z_{max} = \frac{\lambda_{max}}{2} = 0.5\frac{V_{pha_{min}}}{f_{min}} \quad (3)$$

Also, the thickness H_i of the uppermost layer limiting the resolution of subsurface is given in Eq. 4.

$$H_i \geq 0.5\lambda_{min} = 0.5\frac{V_{pha_{min}}}{f_{min}} \quad (4)$$

where:

$Vpha_{max}$ and $Vpha_{min}$ are the maximum and minimum phase velocities of the fundamental mode respectively.

f_{min} and f_{max} are corresponding minimum and maximum frequencies at phase velocity measured.

The maximum wavelength (λ_{max}) is related to the maximum spread length or array length (L), whereas the minimum wavelength (λ_{min}) is related to the minimum distance (2dx) between geophones (O'Neill 2003 in Ezersky et al., 2013).

4. MATERIALS AND METHODS

The field data acquisitions were focused on providing better imaging and characterisation of the subsurface geology through borehole drilling to show the vertical sections of the strata through the collection of ERI and seismic MASW data sets along the seven different profiles. Five parallel profiles that were 5 m away from one another and two diagonal profiles that cut through the five profiles were established. The procedures for the acquisition were presented as follows:

4.1. ERI measurements

The ERI surveys were conducted along seven traverses labelled as T1 to T7 with five parallel traverses trending in approximately S-N direction while the remaining two traverses were taken diagonally across the other five traverses in the SW – NE and SE – NW directions. The parallel profiles have lines spacing of 5 m. The measurements of electrical resistivity were carried out using PASI 16-GL Terrameter connected to four cables (Figure 3) with the Wenner electrode (α) array configuration used. For the Wenner (α) array, the two current electrodes were outside and the two potential electrodes inside with equal inter electrode spacing. The spread lengths for the survey varies between 125– 180 m and a minimum of 5 m to a maximum of 30 m inter-electrode spacing were used along different accessible directions in the study area. The traverses were chosen with a view to having an optimal coverage of the subsurface information. Four standard metallic electrodes (stakes) were used

Figure 3. A PASI electrical resistivity metre for 2D resistivity measurements.

for the resistivity measurements. Two of these electrodes were used as the current electrodes through which current was injected into the ground and the other two electrodes served as the potential electrodes where the resulting potential due to current distribution in the subsurface was measured. For the four cables used, two of which (blue colour) of length of about 500 m each were connected to the current electrodes while the other two cables (red) of short length of about 200 m each were connected to the potential electrodes. A current of 20 mA was injected into the ground. The other survey parameters used were: number of stacks (3); error limits (2.5%); Norm (median). During the data acquisition, no negative resistivity reading was recorded because the electrodes were driven deep into the soils. The measurements started say on traverse 1 in the S-N direction with the four electrodes equally spaced at 5 m, readings proceeded until the end of the traverse was covered. Then, the measurements were repeated for the fixed inter coil spacing of 10 m, 15 m, 20 m, 25 m and 30 m. Again, these steps were taken and repeated on the rest of the traverses. The impedance response of the ground due to the flow of current was averaged and displayed as resistance.

The resistance is measured by injecting an electric current into the ground through a pair of steel stakes (current electrodes) while the resulting potential difference (ΔV) arising from the current flow was measured through another pair of potential electrodes (copper stakes). The response of the ground was estimated as apparent resistivity (ρ) by multiplying the resistance recorded with the geometric factor (k) of the Wenner array using Eqs. 5 and 6.

$$\rho = \frac{2\pi a \Delta V}{I} = 2\pi a R \rho = \frac{2\pi a \Delta V}{I} = 2\pi a R \tag{5}$$

$$\rho = \kappa R \tag{6}$$

where $\kappa = 2\pi a$ = Geometric factor of the electrode configuration

a = electrode spacing

R = resistance of the ground.

To produce an inverted resistivity model, the subsurface is discretized into rectangular blocks. The resistivity model of the subsurface can be obtained by adjusting the apparent resistivity of each block in an iterative way until the difference between the calculated and measured apparent resistivities converged to an acceptable level based on some convergence criteria (Geotomo Software 2009).

Following the field acquisition, the apparent resistivity field (raw) data acquired were converted from text file format into readable format (i.e. .dat) for inversion using the commercially available RES2DINV software package (Loke 2001; Loke et al. 2003). Also, the bad data points were removed before inversion was executed. The software optimised a model of the resistivity distribution of the subsurface under investigation using 2-D finite difference (FD) technique. For the inversion process, both L_1-norm (blocky) and L_2-norm (smoothness) constraints for roughness filter available in the inversion software were tested (Loke et al. 2003). With L_1-norm constraint, the inversion package calculated the mean model residual as the arithmetic mean of the absolute differences between the observed and measured apparent resistivity values. For the L_2-norm, the root mean square (RMS) was calculated during the inversion process iteratively. It was noted that the L_2-norm inversion scheme produced stable resistivity models after a short time as well as smaller RMS error after the fifth iteration and was therefore presented in this study. Table 5 give a summary of the survey parameters used during the inversion process in order to guarantee accurate and reliable resistivity structures. The best resistivity model was selected by successive calculations through iteration process of the model and the data. The model misfit described how close the observed resistivity data was from the measured resistivity data. The model misfit functions for the L_2-norm and L_1-norm are given in by Eqs.7 and 8 respectively as:

$$\emptyset_d(m) = \sum_{i=1}^{N} \left(\frac{\rho_i^{obs} - \rho_i^{mea}}{N} \right)^2 \tag{7}$$

$$\emptyset_d(m) = \frac{1}{N} \sum_{i}^{N} \left| \rho_i^{obs} - \rho_i^{mea} \right| \tag{8}$$

where:

ρ_i^{obs} is the logarithm of observed apparent resistivity

ρ_i^{mea} is the logarithm of measured apparent resistivity

N is the number of observation points

The low error values recorded indicated a good fit and correlation between the result of apparent resistivity measurements and the estimated model of a true resistivity model. In addition to the generated inversion resistivity models, the model cells for sensitivity

Table 5. Inversion processing parameters.

Parameter	Value
Initial damping factor	0.25
Minimum damping factor	0.015
Convergence limit	1
Minimum change in absolute error	<10%
Number of iterations	5
Increase of damping factor with depth	1.05
Robust data inversion constrain is used with cut off factor	0.05
Robust model inversion constrain is used with cut-off factor	0.005
Number of nodes between adjacent electrodes	4
Number of data level	8
Reference resistivity used is the average of minimum and maximum values	1.969

functions were calculated using a robust inversion scheme of the RES2DINV software. The sensitivity values were used to decide the extent to which the errors were randomly distributed.

4.2. MASW measurements

To determine the dynamic physical properties of the soils in the research area, MASW records were also acquired along the seven traverses. On each spread, twenty four (24), vertical component 4.5 Hz geophones were placed on a linear array 48 m long (geophone interval Δx = 2 m). Each geophone was connected via with two multicore cables to the ABEM Mark 6 Terraloc Seismograph. Each geophone was coupled to the ground using 150 mm spikes (Stiebel 2011) and a 9.5 kg sledgehammer was used as impulsive energy source was manually impacted on a rectangular steel plate placed at 2 m offset from the nearest geophone to provide excitation. The roll along technique was deployed for data acquisition with the source-receiver configuration advanced every 2 m after each shot and record along each traverse was taken. The geophones were equally spaced at 2 m (dx = 2 m) resulting in a survey length of 48 m for each spread along the survey traverse as shown in Figure 4. A good subsurface coverage was ensured with a sampling rate of 0.5 ms, given a Nyquist frequency of 1000 Hz (i.e. half maximum frequency). Due to the presence of weak soils that could interrupt the waves during data collection, the number of stacking used was increased from 3 to 7 to improve the signal-to-noise ratio.

The surface waves records (shot gathers) were processed and analysed using Surfseis 4.0 software package from Kansas Geological Survey (KGS) designed to generate a shear wave velocity profile. In the next stage, the dispersion curves/images were generated for the shot gathers recorded in the phase-velocity /frequency mode. This stage was the most critical since it has strongest influence on the confidence level of the shear wave velocity model. The fundamental modes of the Rayleigh waves were chosen only since they were observed to dominate at lower frequency of the dispersion curves. For the inversion process, the dispersion curves were used as the only empirical data without recourse to the original seismic data. The inversion of the estimated dispersion curves used the phase velocity with frequency curve as a reference to determine the shear wave velocity model. The confidence level in the dispersion curves generated was estimated by increasing the signal-to-noise (S/N) ratio. Then, the 1D shear waves velocity models were generated from the inversion of the dispersion curves obtained for each of the twenty-four traces based on Levenberg-Marquardt (LM) global optimisation technique. The LM procedures were based on the linear combination of Gradient descent and Gauss-Newton methods. LM was executed by initialised values for the parameters x, and the damping parameter, λ Then, the residual (r) and the Jacobian (J) for the initial parameter (xo) were evaluated using Eq. 9,

$$\left(jJ^T + \gamma I\right)\delta = J^T r \tag{9}$$

where:

J = Jacobian matrix of derivatives of the residuals with respect to the parameters

λ = damping parameter (adaptive balance between two steps

r = residual vector

The 1D shear wave velocity models obtained were merged into pseudo-2D shear wave velocity models using gradient-based iterative approach. In order to ensure accurate and reliable shear wave velocity models during data processing, dead traces in the field data were edited before transformation was carried out. Also, energy balancing was applied so that the amplitude effects of geometrical spreading and random differences in geophone spacing were accounted for (Lin et al. 2004).

Body waves and the presence of higher modes surface waves were among the factors that might interfere with the analysis of MASW data for accuracy of the dispersion curves. However, their influences were controlled during data acquisition process by ensuring a small offset distance of 2 m (e.g. near offset distance) between the source and the nearest geophone (Park et al. 1999). Furthermore, the spectral content characteristics for both signal and noise waves were examined through the overtone analysis subroutine available on the Surfseis software.

4.3. Analysis of soil strength parameters

The determination of dynamic soil response is of remarkable interest for loads and impacts on the soils. One of the most important parameters in any

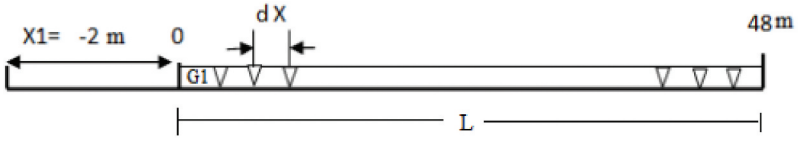

Figure 4. Geometry for MASW data acquisition with array length (L) and geophone spacing (dx) and forward offset shot (X1).

dynamic soil analysis is the shear modulus (G). When foundation vibrations occur usually at very low shear strain levels (i.e. $< 10^{-4}$ %), the shear modulus remains essentially the same (Rollins et al. 1998). The shear modulus has been estimated from in-situ measurements of shear wave velocity (Vs) from seismic surveys. In this work, the shear modulus was estimated using Eq. 9 (Rollins et al. 1998). The density of the soils (ρ) used ranges from (1260– 1470) kg/m^3 depending on soil types.

$$G = \rho Vs^2 \tag{10}$$

More often, it is preferred to determine Vs from in-situ field measurements since it is not feasible economically to take Vs measurements at all points. In the light of this, the use of empirical correlations becomes useful. We used least square regression analysis to establish correlations between the measured resistivity and shear waves velocity values with depths as well as average shear waves velocity and average resistivity measurements along the seven traverse. R-square (R^2) called the coefficient of determination was generated to show the kind of relationship between the measured parameters.

4.4. Geotechnical borehole data

As part of the geotechnical site assessment, validation and constrain to the interpretations of the geophysical data, four boring were drilled (BHs 1– 4) between 10–25 m away from one another in the study area. It is well known that Vs in the upper 30 m of the ground is an important factor for ground characterisation . Therefore, the four boreholes used in this study were drilled down to depths between 35.25 and 45.0 m.

5. RESULTS AND DISCUSSION

5.1. Inverse electrical resistivity models

The 2D inverted resistivity sections which reflect the variations and distribution of resistivity values as function of depth for the investigated wetland area are presented in Fig. 5 (a – g). From the sections, three distinct layers are clearly mapped and classified as low resistivity, intermediate resistivity, and relatively high resistivity regions. It is observed that the resolution of the resistivity models decreases with depth with boundaries in the shallow portion of the models well resolved while deep portions of the models are fairly defined. For all the resistivity sections, the first layer (topsoil) consists predominantly of materials which stretched throughout the model and characterised with low resistivity between 0– 3 Ωm. The average depth is 10 m from the surface of the model. The types and thicknesses of the lithological units (i.e. peat/organic material/silty clay, and sandy clay sediments) assigned to the inverted 2D ERI sections are obtained from the borehole drillings carried out in the site. On correlation with BHs 1, 3 and 4, this layer is made of peat/organic materials/sand filling materials. The second geoelectric layer extends from depths of

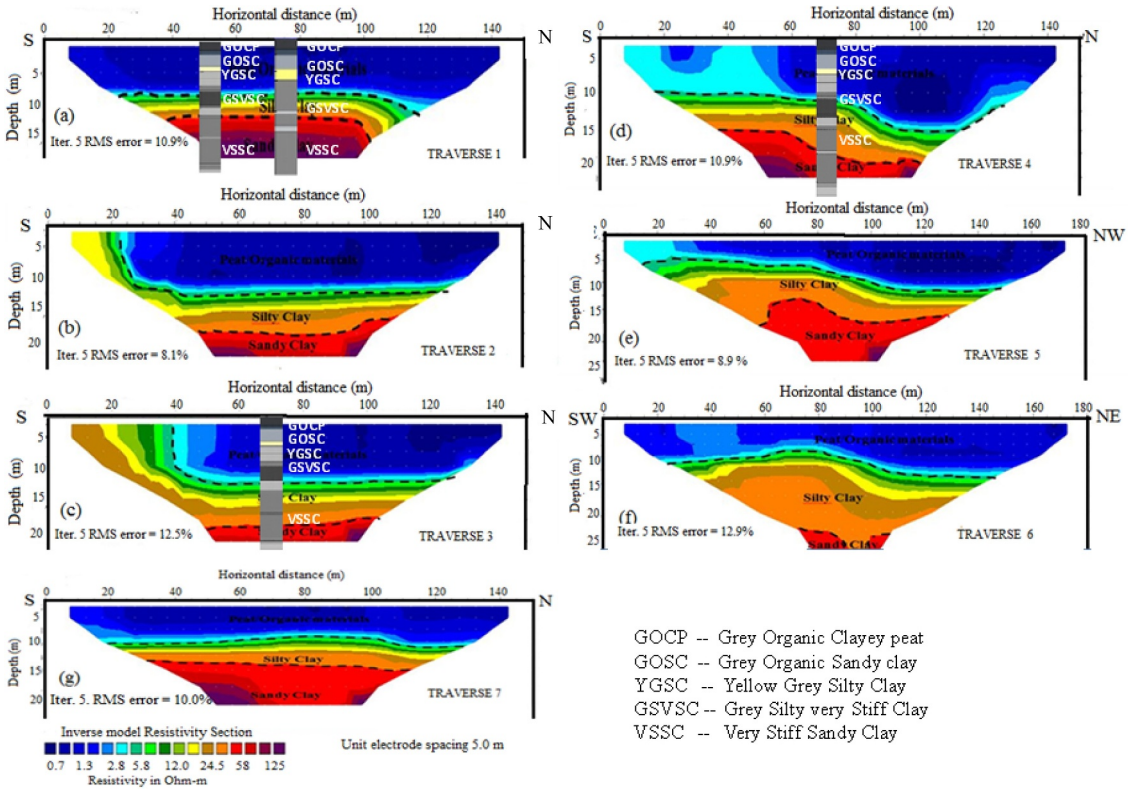

Figure 5. 2D Inverse resistivity sections along the seven resistivity lines.

10.0 to 16.0 m with resistivity ranging from 5– 50 Ω-m and it is identified as an intermediate zone. Using BHs 2 and 3, yellow silty clay to dark grey silty clay geological units was encountered. As a result, the second layer is predominantly of silty clay materials. The ranges of classification conform to the resistivity values for silty clay materials suggested in the work of Ayolabi et al., 2012. The third geoelectric layer is made of material with resistivity in the range of 51–105 Ω-m with thicknesses between 16– 24 m. BHs1, 2 and 4 indicate that the composition is of dark grey sandy clay to very stiff sandy clay. Based on these boreholes log data, the third layer is characterised with sandy clay sediments. This layer represents a partially saturated zone that could conduct water to the peat and silty clay materials above, so could expand and subsequently lead to loss of rigidity. The geotechnical implication of these materials is that they are not suitable for hosting the foundation of engineering structures due to their poor shear strengths. In general, the geology of the subsurface structures mapped in the study area are known from the works of (Jones and Hockey 1964; Omatsola and Adegoke 1981; Longe et al. 1987; Nton et al. 2006; Oyedele and Olorode 2010; Ayolabi et al. 2012). The application of ERI technique has allowed for the identification of these materials and their lateral extents and thus providing an alternative to drilling and mapping of the stratigraphic units.

5.1.1. Image appraisal

Following the 2-D resistivity measurements and processing, image appraisal was deployed to know the regions of the subsurface well captured during the surveys. The sensitivity function/value gives an indirect approach for appraising and evaluating the reliability of the resistivity models (Friedel 2003). The sensitivity values for the inverted resistivity models are presented in Figure 6 (a – g). It is clearly seen that the higher the sensitivity value, the more reliable is the model resistivity value. It shows that the influence of the data set by the individual resistivity of the model cells i.e. the extent to which areas of the imaging region are covered by the data (Kemna 2000). The sensitivity model shows high sensitivity values near the surface with decreasing values as deeper portions of the sections. This is expected since the near surface materials have a greater influence on the measured apparent resistivity values. Also, it is clearly seen that model cells on the edges have greater sensitivities due

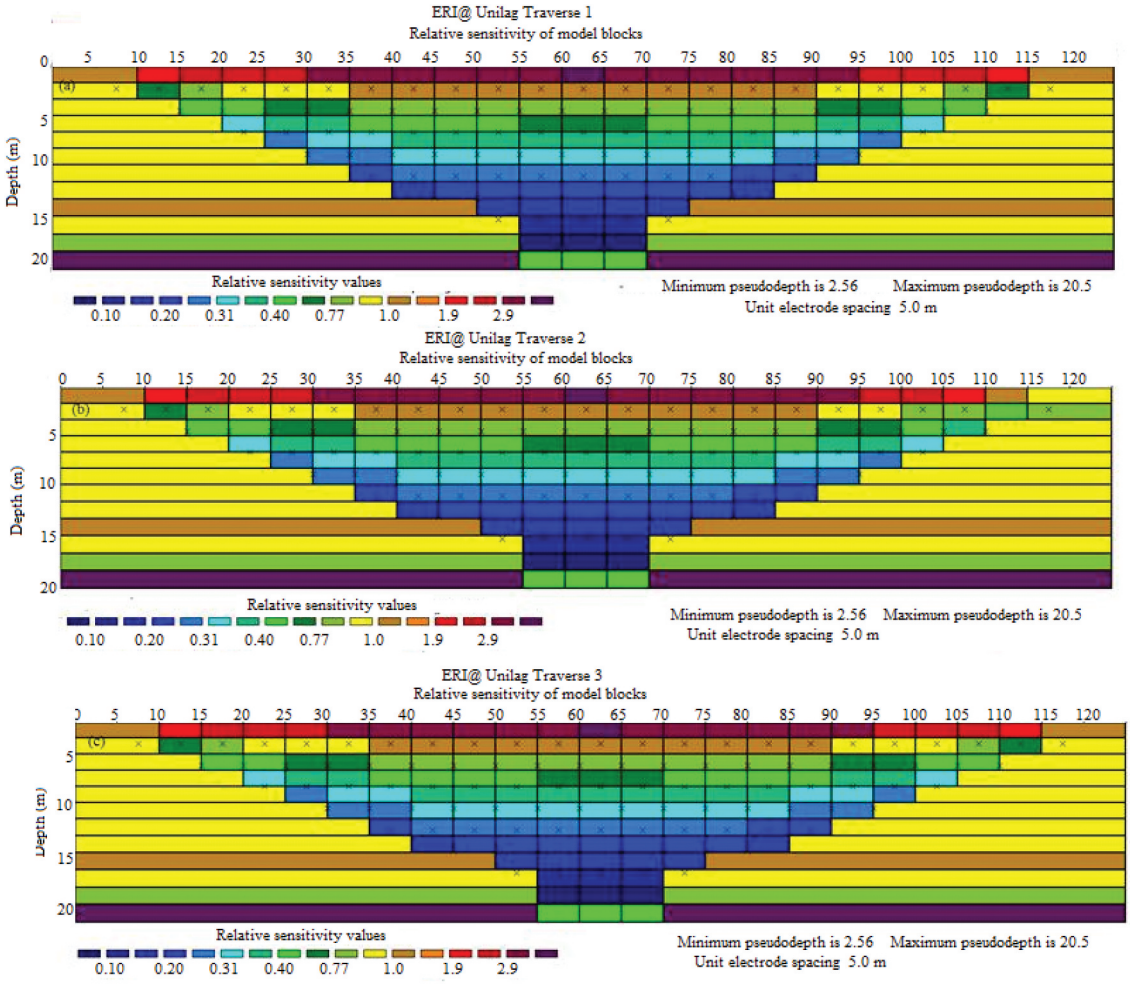

Figure 6. Sensitivity functions of model cells for all traverses.

to large contrasts in resistivity expect for Figure 6(e – g) where the left portion of the models are distorted. This could however be due to the bad data points not properly taking into consideration during data processing.

5.2. Shear wave velocity models

Typical shot gathers acquired by the MASW technique with strong ground roll component energy without much interference from body wave or air wave (cultural noise) are shown in time-space domain as Figure 7 (a – b). The air wave event is seen clearly as separate

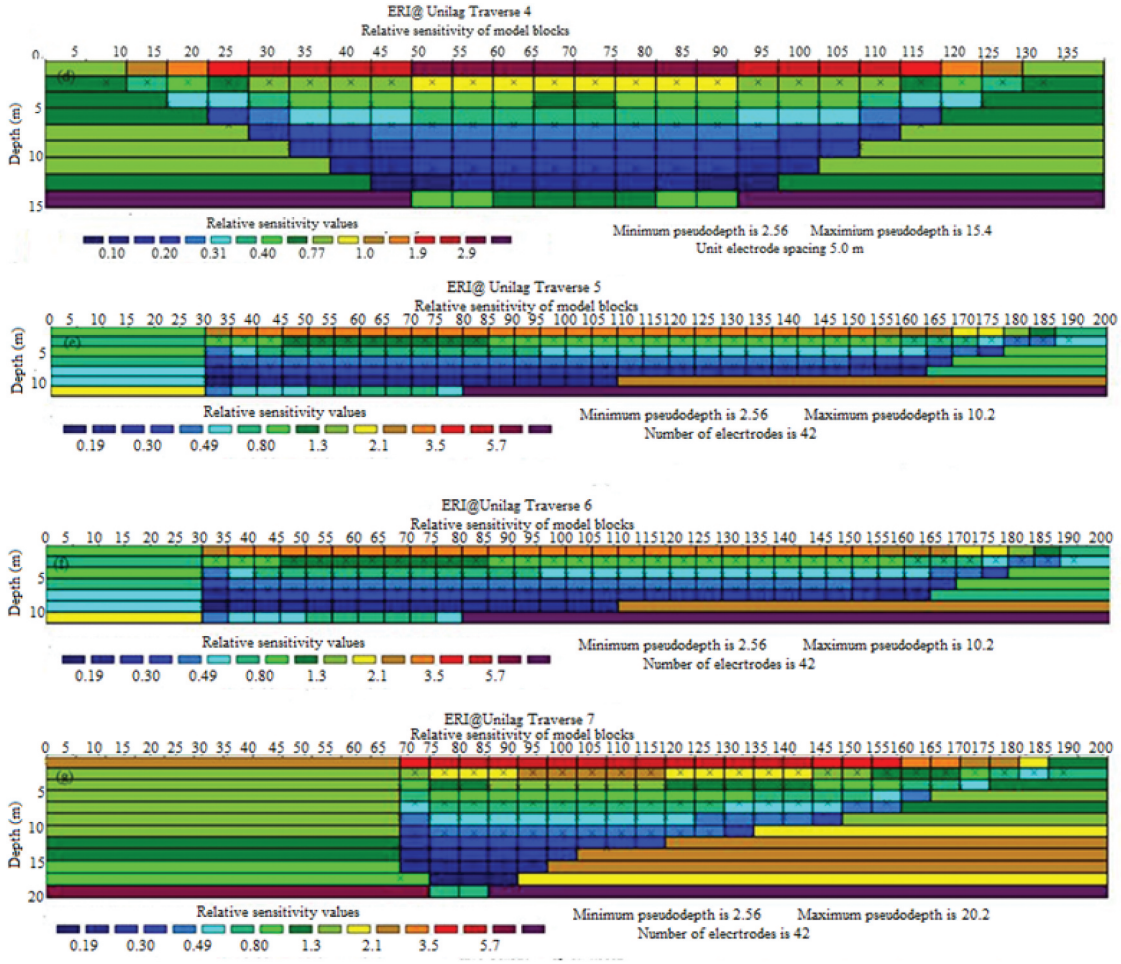

Figure 6. Continued.

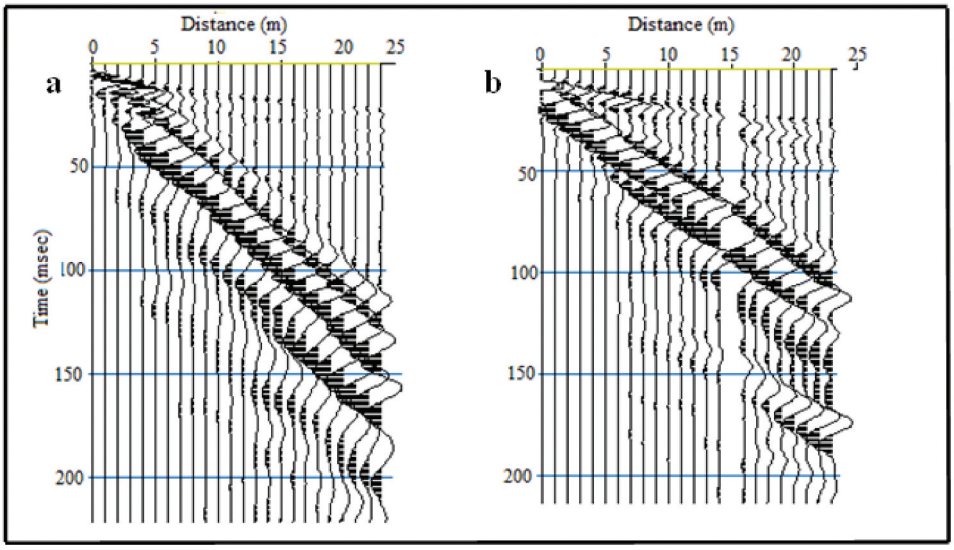

Figure 7. Twenty-four channel shot gathers for Rayleigh waves in the time-space domain.

event from the surface wave with much less energy. Also, representative dispersion curves/images for the MASW measurements are shown in Figure 8 (a – c). The dispersion images show the (f – v) spectrum and the maximum peaks at a given frequency. In addition, separate modes which consist of the fundamental characterised with low frequency, the first and second higher modes are clearly seen. The signal to noise ratio is between 0.4 and 0.8. Each 1D profile (not shown) is inverted to give the 2D shear wave velocity models. No lateral constraints were applied during inversions since surface wave dispersion stacking naturally smoothened the data. The 2D shear waves velocity (Vs) models for the seven traverses obtained from the analysis of MASW field data are shown in Figure 9 (a – g). In contrast to the inverted resistivity models where the physical parameter used to characterise the subsurface is the resistivity values, the velocity distribution is the physical parameter used in surface wave models. Visual inspection of inverted Vs models shows that three distinct layers are mapped with general increase in Vs with depth. This suggests a good resemblance with the inverted resistivity models. The depth of investigation obtained is in the range of 25 to 35 m. In some of Vs models, perturbation of the high-velocity layers by low-velocity layers is clearly observed too. This could reflect the unstable nature due to low compactness of the soils beneath the investigated area. The velocity sections show that Vs varies from 25 m/s at the surface to 150 m/s in the deepest part of the sections. The closeness of these inverted models in spite of the uncertainties arising from non-uniqueness of inversion models and the smearing effect that characterises especially the surface wave analysis underscores the choice of the integrated approach used in this study. The borehole data collected prior to the geophysical surveys provided the baseline for identification and delineation of the various strata. For the Vs models, the first layer the top soil is made of material characterised with low Vs in the range of 25– 70 m/s (blue/blue with white patches colour) with oscillating thicknesses from the ground surface. This layer consists of peat/organic materials (Adegbola et al. 2016). Also, an intermediate zone which sandwiches the overburden and underlying layers is delineated and it is characterised with materials of Vs that spans between 75– 110 m/s. It is representative of silty-clay sediments. The third layer is clearly observed and well resolved too in the deepest portion of the sections. The velocity for this zone ranges from 120– 150 m/s and it is characteristics of sandy clay sediments. This result corroborates one of the advantages of MASW over ERI techniques. The variations in the values of Vs could be due to changes in lithological units. The range of Vs obtained for the three geological units mapped in this study agrees well with the earlier works (Oyedele and Olorode 2010; Ayolabi et al. 2012; Adegbola et al. 2016; Adeoti et al. 2018). The peat/organic materials are seen to thicken towards the northern end of the profiles while for the rest of the images, the geo-materials trend ES-NW direction. The reliability of the Vs models generated is good and assured due to careful selection of the survey parameters used. In this study, the depth of investigation obtained is due to the low frequency geophones used. Also, we used all available information for the parameterisation of the initial model prior to inversion. This becomes necessary to minimise the non-uniqueness inherent in the inversion process. The Vs values obtained and the lithologic units assigned to each layer are consistent with the borehole log data.

5.3. Borehole investigations data

The four borehole logs (BHs 1– 4) for the study site used for validation of the geophysical data are shown in Figures 10 and 11. It should be noted that Figure 9 is a representation of a single geotechnical drilling while Figure 11 is a collection of the drilled boreholes given a fair representation of the geological formation in the investigated area. During the drilling campaign, BH-1 was drilled to a depth of about 33 m while BHs-2, 3 and 4 were drilled to depths approximately 44 m. For BH-1, the first zone encountered in the borehole stratigraphic column reveals dark grey organic clayey peat at depth of 0– 2.25 m. This layer could be ascribed to having low shear strength and high compressibility. The second stratum is encountered at depth between 3– 3.75 m is composed of dark grey organic sandy clay. The third layer is of dark grey silty clay material drilled to a depth of 3.75– 7.5 m. The fourth layer encountered reveals yellowish grey silty clay at depth of 7.5– 10.5 m. The fifth unit encountered reveals multi grey silty very stiff clay at depth of 10.5– 18.0 m. The sixth and seventh strata also reveal multi grey silty sandy clay and multi grey silty very stiff clay at depths of 18– 18.75 m and 18.75– 21.75 m respectively. The eighth and ninth units encountered show very stiff silty sand clay and multi- grey silty very stiff clay at depths of 21.75– 23.25 m and 23.25–33.25 m respectively. It is observed that there is a close resemblance in the compositions of the BHs-2, 3, and 4 with BH-1 with slight alternation in strata.

5.4. Engineering implications of the geological structures mapped

The soil behaviour in terms of strength and density which are used for foundation design depends on the water contents in the soils. The silty soils delineated as part of the materials in this study, are non-plastic fine soils and mostly unstable in the presence of water and like fine sands often become problematic quick soil. A method of treating the silty soils in normal

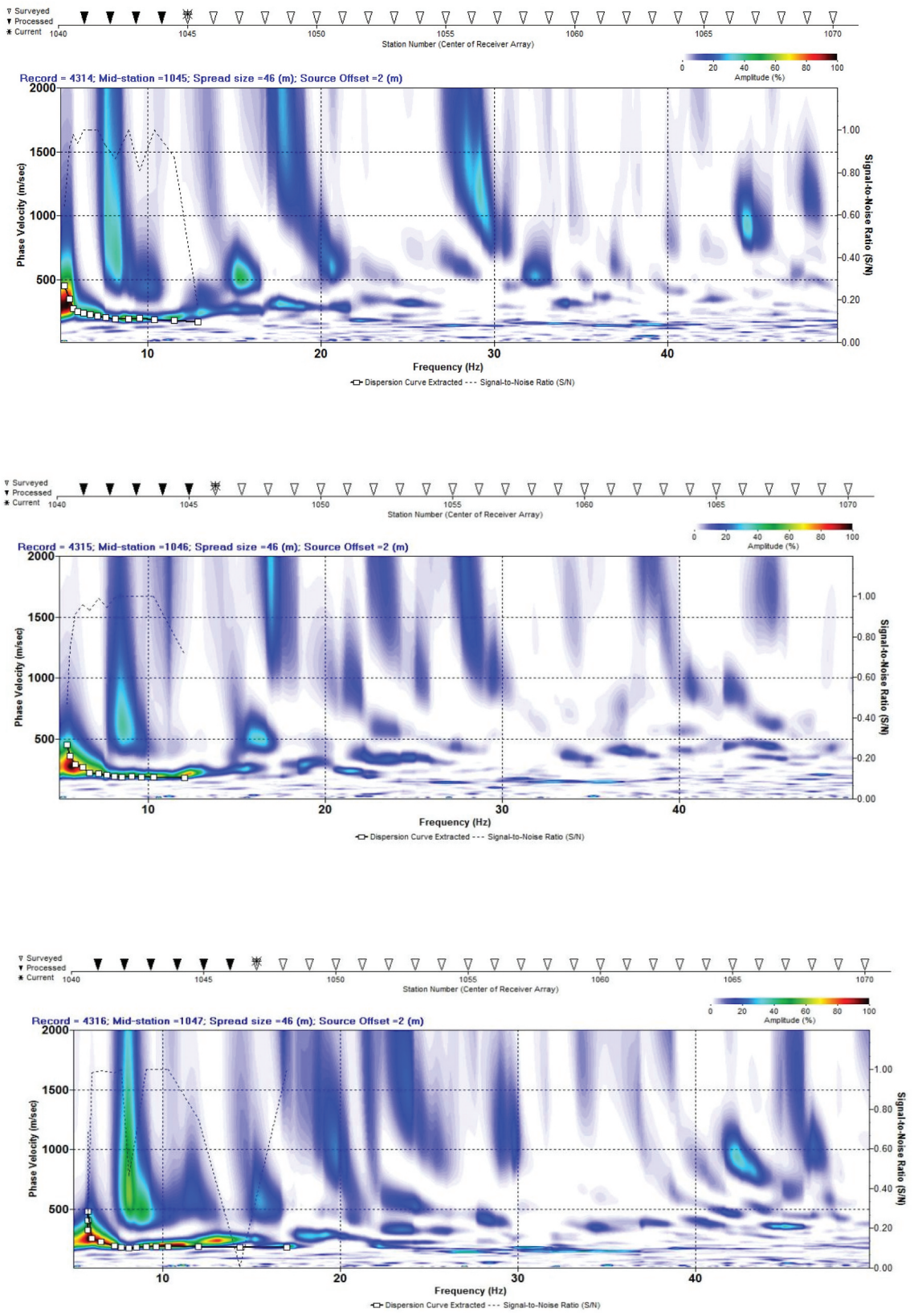

Figure 8. (a-c) Dispersion images for Rayleigh waves showing fundamental and higher modes.

foundation engineering design is to prevent subjecting the silty soils to load by driving piles through them to firm underlying strata.

The silt and clay soils may be subjected to undesirable changes in deformation and strength properties even when not being loaded. This is because the silt and clay soils have low plasticity, low density, and high water content making them more apt to cause such problems to earth structures and foundations.

Clay soils are prevalent in coastal, floodplains, and deltas areas. As a result, the use of clay soils as engineering structural materials is limited because of their

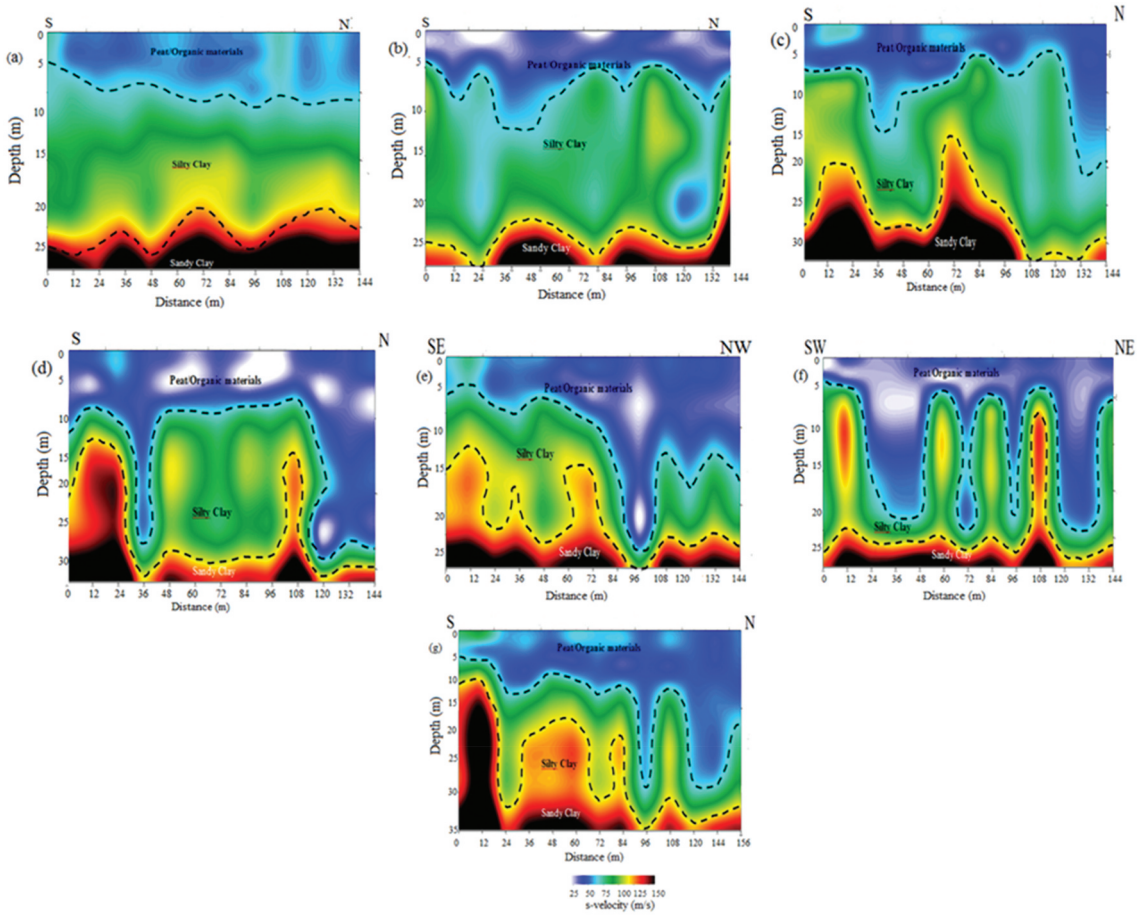

Figure 9. (a – g) Shear wave velocity models from MASW surveys along the seven traverses.

relatively high water content, great capacity for compressibility, and low bearing capacity. Some clay minerals can reduce bulk resistivities of rocks through the release of exchangeable cations to the pore fluid. Related studies conducted in some other parts of the wetland area of Lagos have shown that the clays sediments become expansive soils when saturated. As a result, it could set up strong mechanical stresses on underlying materials leading to fracture or shear zone. This zone may reduce the bearing capacity of the strata or serve as conduct for movement of surface or groundwater. These soils pose problems to foundation and settlement of structures as a result are unfit for hosting the foundation footings for the substantial engineering structures along the entire traverses investigated.

5.5. Correlation of ERI and MASW results

Correlation of measured model parameters (i.e. resistivity and velocity) with depth and the inferred lithology is presented in Table 6. On a comparison, a reasonably correlation is observed in the trends and curvatures of the ERI and MASW profiles. Another notable feature is the regions of low resistivity and low shear wave velocity in both ERI and MASW sections. These regions suggest the prevalence of peat and silty clay sediments within the study area. The ERI results show that resistivity variations within the range of 0.7– 105 Ωm along the seven traverses. The MASW results also indicated that the shear wave velocity varies between 25– 150 m/s, characteristics of very soft soil layers of low shear strengths. The estimated shear moduli for the three classes of geological layers (i.e. peat/organic materials/silty clay/sandy clay) delineated are in the range of 1.25– 45.0 MPa is presented in Table 7. For the low velocity layer, the average shear modulus is 5.5 MPa while the average shear modulus for the relatively high velocity layer is 73.8 MPa. In this study, the shear modulus for the sandy clay formation is about 15 times its values for the peat/organic materials.

5.6. Analysis of electrical resistivity/shear wave velocity with depth correlations

The plots of electrical resistivity and shear wave velocity (Vs) with depth along the seven traverses for the investigated site are shown in Figure 12 (a – g). The plots all show positive correlations between the measured parameters. The R-squared values for Vs against depth are in the range of 0.64 to 0.98 while the R-squared values for electrical resistivity

Figure 10. Stratigraphic column of BH 1 drilled within the study area.

(ρ) against depth fall between 0.87 and 0.96. According to Jusoh and Osman (2017) these values correspond to moderate, strong ad very strong correlations. The regression model for the average Vs and resistivity ρ is shown in Figure 12h. According to this figure, the regression equation for this correlation is: $V_s = 1.17\rho + 45.69$. The R-squared of 0.92 indicates very strong correlation. This demonstrates that the regression model could be used to predict the shear waves velocity (Vs) from the resistivity measurements when in-situ surface wave measurements are not carried out.

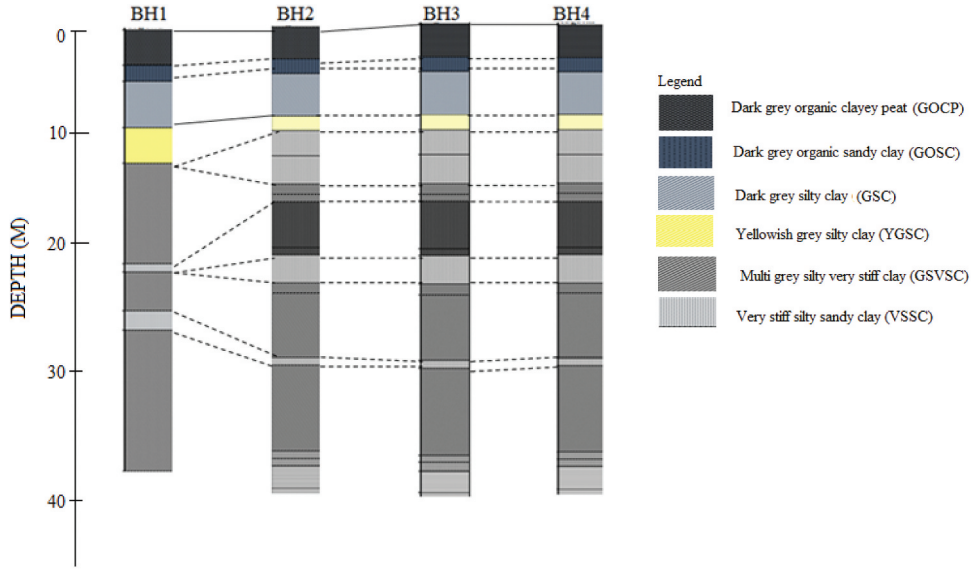

Figure 11. Generalised stratigraphic columns for the four boreholes (BHs 1–4) drilled within the study.

Table 6. Typical resistivity, S-wave velocity value range for different lithological units at the study area.

		ERI section		MASW section		
Traverse	Layer	Average Depth Range (m)	Resistivity (ρ) (Ω-m)	Depth (m)	Shear Wave velocity (Vs) (m/s)	Inferred Lithology
1	1	0– 10	0.7– 3	0– 6	25– 70	Peat/organic material
	2	10– 16	5– 50	6– 13	70– 120	Silty clay
	3	16– 24	51– 105	12– 14	120– 150	Sandy clay
2	1	0– 12	0.7– 3	0– 11	25– 70	Peat/organic material
	2	12– 21	5 –50	11– 25	70– 120	Silty clay
	3	21– 24	51– 105	25– 28	120– 150	Sandy clay
3	1	0– 13	0.7– 3	0– 11	25– 70	Peat/organic material
	2	13– 21	5– 50	11– 20	70– 120	Silty clay
	3	21– 24	51– 105	20– 33	120– 150	Sandy clay
4	1	0– 13	0.7– 3	0– 15	25– 70	Peat/organic material
	2	10– 20	5– 50	5– 15	70– 120	Silty clay
	3	15– 24	51– 105	15– 16	120– 150	Sandy clay
5	1	0– 12	0.7– 3	0– 12	25– 70	Peat/organic material
	2	7– 20	5– 50	5– 12	70– 120	Silty clay
	3	20– 34	51– 105	12– 14	120– 150	Sandy clay
6	1	0– 15	0.7– 3	0 –17	25- –70	Peat/organic material
	2	8– 29	5– 50	5– 20	70– 120	Silty clay
	3	29– 34	51– 105	20– 24	120– 150	Sandy clay
7	1	0– 10	0.7– 3	0– 10	25– 70	Peat/organic material
	2	10– 15	5– 50	4– 12	70– 120	Silty clay
	3	15– 24	51– 105	12– 14	120– 150	Sandy clay

Table 7. Estimated Shear modulus of soil from MASW data.

Shear waves velocity (Vs) m/s	Material Status	Shear Modulus (G) MPa	Inferred Lithology
25 –70	Low velocity layer (LVL)	1.25– 9.8	Peat/Organic materials
70– 120	Medium velocity layer (MVL)	9.8– 28.8	Silty clay
120– 150	High velocity layer (HVL)	28.8– 45.0	Sandy clay

6. CONCLUSIONS

An application of integrated approach for subsurface characterisation has helped to develop geophysical models of the Earth as alternative to the conventional drilling tests techniques. For the inverted resistivity sections, the near surface structures were better resolved at shallow depth while the shear waves velocity models, structures at deeper portion of the sections were well resolved. This underscores the complementary nature of the investigated techniques used in this study. In both sections, three strata with variations in resistivity and shear waves velocity values were identified and mapped. The first layer (topsoil) is characterised with resistivity and velocity values of 0.7– 3 Ωm and 25– 70 m/s respectively. This layer is composed of loose soil or less compacted peat/organic materials. The underlying layer is having resistivity values of 5– 50 Ωm and shear wave velocity values that spans between 70– 120 m/s. It is representative of silty clay.For the third layer, the resistivity varies between 51– 105 Ωm and shear wave velocity

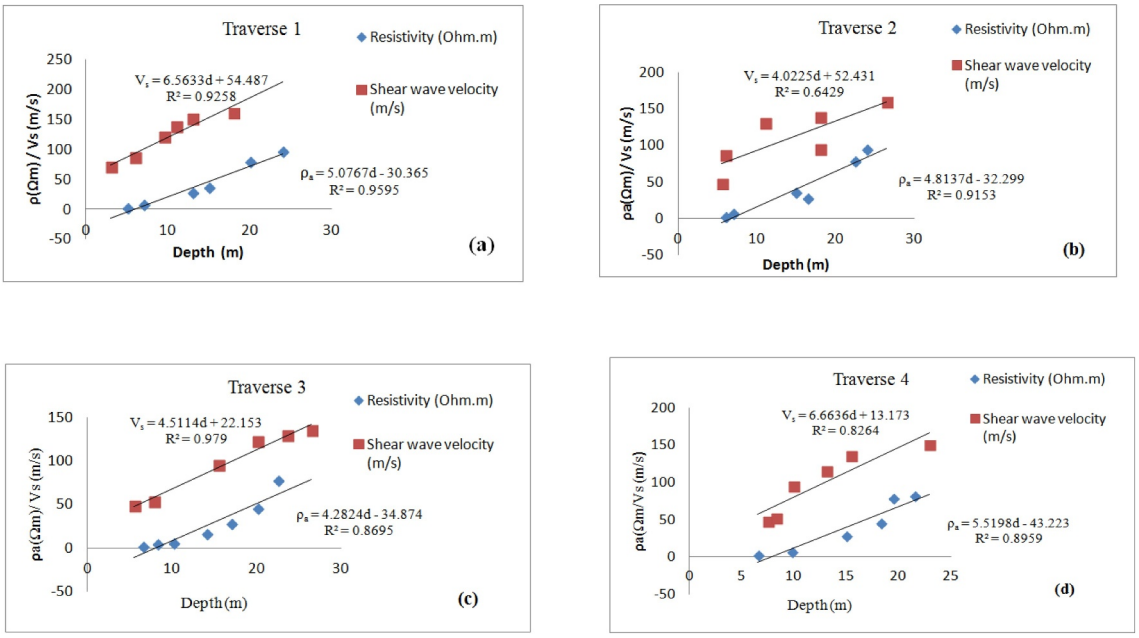

Figure 12. Variations of resistivity and Vs with depth for (a) traverse 1 (b) traverse 2 (c) traverse 3 (d) traverse 4 (e) traverse 5 (f) traverse 6 (g) traverse 7 and (h) correlation between average velocity vs average resistivity.

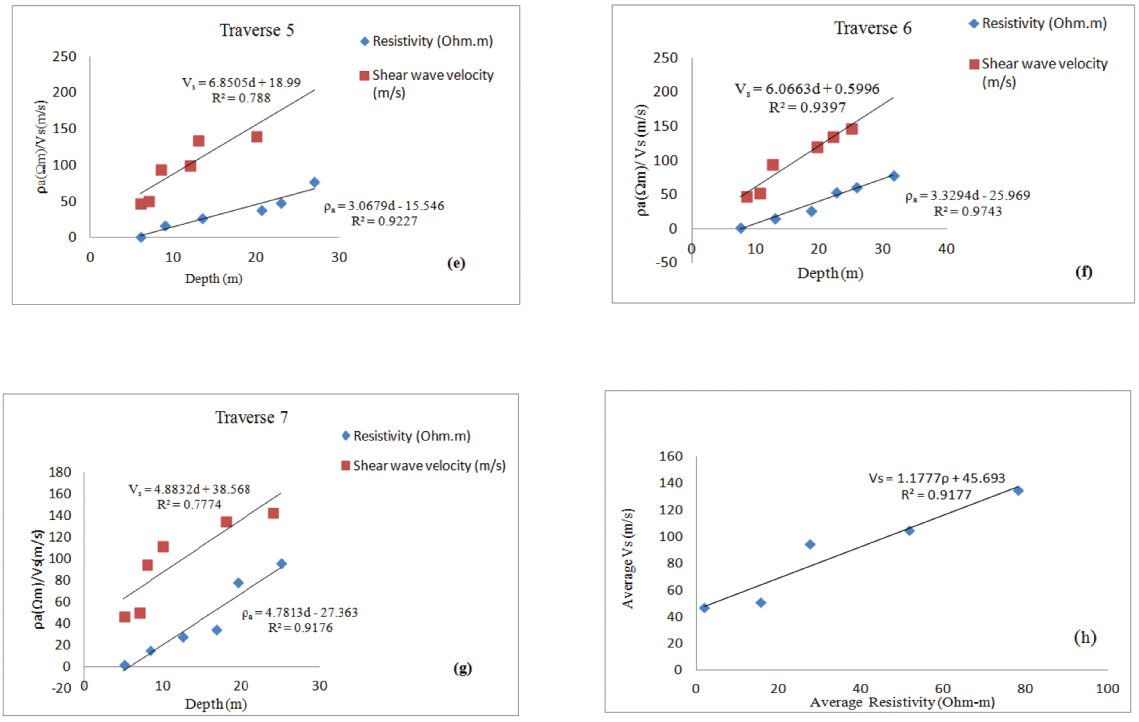

Figure 12. Continued.

values of 120– 150 m/s. The composition of this layer is sandy clay sediments. The variations in resistivity and velocity could be due to change in lithological units. The empirical relationships established for the measured parameters using least square regression analysis show moderate to very good correlations. The peat/organic materials, silty clay/sandy clay units that dominates then area have relatively low shear strengths and more plastic. Consequently, these earth materials become problem due to water content. Under this condition, these soils are susceptible to uneven settlement when loaded or stressed. The site is characterised with weak/incompetent strata with depth to competent layer possibly greater than the depth investigated in this study. Deep foundation through pilling to the competent layer is to be given attention on the study area. In addition, soils treatment

is suggested for improving the strength and stability of the soils. This will substantially improve the bearing capacity of the soils in the investigated area.

Disclosure of potential conflicts of interest

No potential conflict of interest was reported by the author(s).

ORCID

K.S. Ishola http://orcid.org/0000-0002-2915-157X

References

Adegbola RB, Oyedele KF, Adeoti L, Adeloye AB. 2016. Multichannel analysis of the surface waves of earth materials in some parts of Lagos State, Nigeria. RMZ – M&G. 63:81–90.

Adegoke OS, Jeje LK, Durotoye B, Adeleye DR, Ebukanson EE. 2010. The geomorphology and aspects of sedimentary of Coastal Region of Western Nigeria. Journal Min. Geo. 17: 217–223

Adeoti L, Opene-Odili PN, Oyedele KF, Oyeniran TA, Ishola KS, Ayuk MA. 2018. Exploring the linkages between geophysical and geotechnical prospection to detect foundation failure of buildings in a Wetland Area of Lagos, Southwestern Nigeria. Nigerian Research Journal of Engineering and Environmental Sciences. 3(1):416–427.

Adiat KAN, Akinlalu AA, Adegoroye AA. 2017. Evaluation of road failure vulnerability section through integrated geophysical and geotechnical studies. NRIAG Journal of Astronomy and Geophysics. 6(1):244–255. doi:10.1016/j.nrjag.2017.04.006

Aggelis DG, Shiotani T. 2007. Experimental study of surface wave propagationin strongly heterogeneous media. J Acoust Soc Am. 122(5):5. doi:10.1121/1.2784151

Ajibola MO, Adewale BA, Ijasan KC. 2012. Effects of Urbanization on Lagos Wetlands: International Journal of Business and Social Science. 3(17):310–318.

Amini A, Ramazi H. 2016. Application of electrical resistivity imaging for engineering site investigation. A case study on prospective hospital site, Varamin, Iran. Acta Geophys. 64(6):2200. doi:10.1515/acgeo20160100

Anderson N, Hoover R, Sirles P. 2008. Geophysical methods commonly employed for geotechnical site characterization. Transportation Research Broad of the National Academies E-C 130. 2008:43.

Arjwech R, Everett ME. 2015. Application of 2D electrical resistivity tomography to engineering projects: three case studies. Songklanakarin J. Sci Technol. 37(6):675–681.

Ayedun CA, Durodola OD, Akinjare OA. 2012. An empirical ascertainment of the causes of building failure and collapse in Nigeria. Mediterranean Journal of Social Sciences. 3(1):313–322.

Ayolabi EA, Folorunso AF, Jegede OE. 2012. An application of 2D electrical resistivity tomography in geotechnical investigations of foundation detects: a case study. Journal of Geology and Mining Resources. 3(12):142–151.

Bakir S, Sucuoglu H, Yilmaz T. 2002. An overview of local site effects and the associated building damage in adapazari during the 17 August 1999 Izmit Earthquake. Bulletin of the Seismological Society of America (BSSA). 92 (1):509–526. doi:10.1785/0120000819

Båth M. 1973. Introduction to seismology: A Halsted Press Book, p. 395.

Chambers JE, Wilkinson PB, Uhlemann S, Sorensen JPR, Roberts C, Newell AJ, Ward WOC, Binley A, Williams PJ, Gooddy DC, et al. 2014. Derivation of lowland riparian wetland deposit architecture using geophysical image analysis and interface detection. Water Resour Res. 50 (7):5886–5905. doi:10.1002/2014WR015643

Chendo IG, Obi NI. 2015. Building collapse in Nigeria: the causes, effects, consequences and remedies. International Journal of Civil Engineering, Construction and Estate Management. 3(4):41–49.

Comas X, Slater L, Reeve A. 2004. Geophysical evidence for peat basin morphology and stratigraphic controls on vegetation observed in a Northern Peatland. J Hydrol. 295(1–4):173–184. doi:10.1016/j.jhydrol.2004.03.008

Dahlin T, Zhou B. 2006. Multiple-gradient array measurements for multichannel 2D resistivity imaging. Near Surface Geophysics. (2):113–123. doi:10.3997/1873-0604.2005037

Desta H, Lemma B, Fetene A. 2012. Aspects of climate change and its associated impact on wetland ecosystems- A review. Journal of American Science. 8(10):582–596.

Dobry R, Borcherdt RD, Crouse CB, Idriss IM, Joyer WB, Martin GR, Power MS, Edwards LS. 1977. A modified pseudosection for resistivity and IP. Geophysics. 42 (5):1020–1036. doi:10.1190/1.1440762

Evrett ME. 2013. Near-surface Applied Geophysics. Cambridge: Cambridge University Press.

Foti S, Sambuelli L, Valentina LS, Strobbia C. 2003. Experiments of joint acquisition of seismic refraction and surface wave data. Near Surface Geophysics. (3):119–129. doi:10.3997/1873-0604.2003002

Friedel S. 2003. Resolution, stability and efficiency of resistivity tomographyestimated from a generalized inverse approach. Geophys J Int. 153(2):305–316. doi:10.1046/j.1365-246X.2003.01890.x

Gebhardt H, Adekeye OA, Akande SO. 2010. Late paleocene to initial eocene thermal maximum foraminifera biostratigraphy and paleoecology of the Dahomey Basin, southwestern. Jahrbuch der Geologischen Bundesansalt, 150: 407–419.

Geotomo Software. 2009. Res2dinv ver. 3.55 Manual. Geotomo Software, Malaysia.

Gharibi M, Bentley LR. 2005. Resolution of 3-D electrical resistivity images from inversions of 2-D orthogonal lines. Journal of Environmental and Engineering Geophysics. 10(4):339–349. doi:10.2113/JEEG10.4.339

Giang NV, Duan NB, Thanh L, Hida N. 2013. Geophysical techniques to aquifer locating and monitoring for industrial zones in North Hanoi, Vietnam. Acta Geophys. 61 (6):1573–1597. doi:10.2478/s11600-013-0147-8

Giao P, Chung S, Kim D, Tanaka H. 2003. Electric imaging and laboratory resistivity testing for geotechnical investigation of pusan clay deposits. J Appl Geophys. 52 (4):157–175. doi:10.1016/S0926-9851(03)00002-8

Grandjean G, Pennetier C, Bitri A, Meric O, Malet JP. 2006. Caracterisation de la structure interne et de l'e´tat hydrique de glissements argilo-marneux par tomographie ge´ophysique: l'exemple du glissement-coule´e de supersauze (Alpes du Sud, France). CR Geosci. 338 (9):587–595. doi:10.1016/j.crte.2006.03.013

Hill MB, Webb JE. 1958. The topography and physical features of lagos harbour. Phil Trans R Soc (Series B). 241:319–333.

Ishola KS, Nawawi MNM, Abdullah K. 2014. Combining multiple electrode arrays for two-dimensional electrical

resistivity imaging using the unsupervised classification technique. Pure and Applied Geophysics. 172 (6):1615–1642. doi:10.1007/s00024-014-1007-4
Jones HA, Hockey RD. 1964. The geology of part of south-western Nigeria. Geological Survey of Nig Bull. 31:101.
Jusoh H, Osman SBS. 2017. The correlation between resistivity and soil properties as an alternative to soil investigation. Indian J Sci Technol. doi:10.17485/ijst/2017/v10i6/111205
Kearey P, Brooks M, Hill I. 2002. An Introduction to Geophysical Exploration. London: Blackwell Science Ltd.
Kemna A. 2000. Tomographic Inversion of Complex Resistivity: theory and Application. Osnabrück: Der Andere Verlag.
Kettridge N, Comas X, Baird A, Slater L, Strack M, Thompson D, Jol H, Binley A. 2008. Ecohydrologically important subsurface structures in peatlands revealed by ground-penetrating radar and complex conductivity surveys. J Geophys Res. 113(G4):G04030. doi:10.1029/2008JG000787
Kowalczyk S, Zawrzykraj P, Maślakowski M. 2017. Application of the electrical resistivity method in assessing soil for the foundation of bridge structures: a case study from the warsaw environs, Poland. Acta Geodyn Geomater. 14(2):221–234. doi:10.13168/AGG.2017.0005
Lai CG, Wilmanski K. 2005. Surface waves in geomechanics: direct and inverse modeling for soils and rocks. Udine (Italy): International Centre for Mechanical Sciences. CISM Courses and Lectures No. 481.
Lapenna V, Lorenzo P, Perrone A, Piscitelli S, Sdao F, Sdao F. 2003. High-resolution geoelectrical tomographies in the study of the giarrossa landslide (Potenza, Basilica-ta). Bull Eng Geol Environ. 62(3):259–268. doi:10.1007/s10064-002-0184-z
Lin C, Chang C, Chang T. 2004. The use of MASW method in the assessment of soil liquefaction potential. Soil and Earthquake Engineering. 24(9–10):689–698. doi:10.1016/j.soildyn.2004.06.012
Loke MH. 2001. Tutorials: 2-D and 3-D Electrical Imaging Surveys. Penang, Malaysia.
Loke MH, Acworth I, Dahlin T. 2003. A comparison of smooth and blocky inversion methods in 2D electrical imaging surveys. Explor Geophys. 34(3):182–187. doi:10.1071/EG03182
Longe EO, Malomo S, Olorunniwo MA. 1987. Hydrogeology of Lagos metropolis. Journal of African Earth Sciences. 1983, 6(2):163–174. doi:10.1016/0899-5362(87)90058-3. Hill.
Maltby E. 2009. The Changing Wetland Paradigm. In: Maltby E, Barker T, editors. The Wetland Handbook. Oxford (UK): Wiley-Blackwell; p. 3–42.
Mansoor N, Slater L. 2007. Aquatic electrical resistivity imaging of shallow-water wetlands. Geophysics. 72(5): F211– F221. doi:10.1190/1.2750667
Mckinley JM, Worden RH, Ruffell AH. 2003. Smectite in sandstones: a review of the controls on occurrence and behaviour during diagenesis. Int Assoc Sedimentol Spec Publ. 34:109–128.
Nath SK 2008. Seismic microzonation framework-principles and applications. Proc., Workshop on Microzonation, Indian Institute of Science, Bangalore, 26/27, 9–35.
Nigeria Meteorological Agency (NIMET). 2007. Daily weather forecast on the Nigerian Television Authority. Oshodi (Lagos):Nigerian Metrological Agency.
Nton ME, Eze FP, Elueze AA. 2006. Aspects of source rock evaluation and diagenetic history of the akinbo shale, eastern Benin basin, southwestern Nigeria. Niger Assoc Petroleum Geol Bull. 19(1):35–49.
O'Neill A 2003. Full-waveform reflectivity for modeling, inversion and appraisal of seismic surface waves dispersion in shallow site investigations. Ph.D Thesis. Geophysics.
Olagunju RE, Aremu SC, Ogundele J. 2013. Incessant Collapse of Buildings in Nigeria: Journal of Civil and Environmental Research. 5790 and 2225–0514, 3(4), 49–54.
Olatinsu OB, Oyedele KF, Ige-Adeyeye AA. 2018. Electrical resistivity mapping as a tool for post-reclamation assessment of subsurface condition at a sandfilled site in Lagos, southwest Nigeria. SN Applied Sciences. 1(1):24. doi:10.1007/s42452-018-0028-5
Olusola BS, A K I N T A Y O O. 2009. An assessment of failure of building components in Nigeria. Journal of Building Appraisal. 4(4):279–286. doi:10.1057/jba.2009.6
Omatsola ME, Adegoke OS. 1981. Tectonic evolution and Cretaceous stratigraphy of the benin basin. J Min Geol. 18 (1):130–137.
Oyedele, KF, Oladele, S, and Okoh, C. (2015). Assessments of subsurface conditions in a coastal Area of Lagos using Geophysical methods. Nigerian Journal of Technological Development, 12(2), 36–41.
Oyedele KF, Olorode DO. 2010. Site investigations of subsurface conditions using electrical resistivity method and cone penetration test at medina estate, Gbagada, Lagos, Nigeria. World Applied Sciences Journal. 11 (9):1097–1104.
Oyediran IA, Famakinwa JO. 2015. Geotechnical basis for building instability and failure: case study from Lagos, Nigeria. In: Engineering Geology for Society and Territory. Cham: Springer. 5; p. 365–370. doi: 10.10007/978-3-09048-1_70
Pacanowski G, Czarniak P, Bąkowska A, Mieszkowski R, Welc F. 2014. The role of geophysical ERT method to evaluate the leakproofness of diaphragm wall of deep foundation trenches on the example of the construction of retail and office complex in Lublin, Poland. Studia Quaternaria. 31(2):91–99. doi:10.2478/squa-2014-0009
Papadopoulos N, Tsourlos P, Tsokas G, Sarris A. 2006. Two dimensional and three dimensional resistivity imaging in archaeological investigation archaeol. Prospect. 13:163–181.
Park, CB, Xia, J, Miller, RD. 1998. Surface waves as a tool to image near-surface anomaly: 68th Ann. Internat. Mtg. Soc.Expl.Geophys., Expanded Abstracts, 874–877.
Park CB, Miller RD, Xia J. 1999. Multichannel analysis of surface waves. Geophysics. 64(3):800–808. doi:10.1190/1.1444590
Popp S, Altdorff D, Dietrich P. 2013. Assessment of shallow subsurface characterisation with non-invasive geophysical methods at the intermediate hill-slope scale. Hydrol Earth Syst Sci. 17(4):1297–1307. doi:10.5194/hess-17-1297-2013
Pugh JC. 1954. A classification of the Nigerian Coastaline. J W African Sci. 1:3–12.
Rezaeian M, Gruen A. 2007. Automatic classification of collapsed buildings using object and image spacefeatures. In: Li J, Zlatanova S, Fabbri A, editors. Geomatics solutions for Disaster Management. Springer; p. 135–148. Springer, Berlin, Heidelberg.
Rix GJ, Leipski AE. 1991. Accuracy and resolution of surface wave inversion. In: Bhatia SK, Blaney GW, editors. Recent advances in instrumentation, data acquisition and testing in soil dynamics. 28. Geotechnical Special

Publication; Am.Soc. Civil Eng, p. 17–23. American Society of Civil Engineers.

Rollins KM, Evans MD, Diehl NB, Daily III WD. 1998. Shear modulus and damping relationships for gravels. Journal of Geotechnical and Geoenvironmental Engineering. 124(5):396–405. doi:10.1061/(ASCE)1090-0241(1998)124:5(396)

Shemang EM, Molwalefhe LN. 2009. DC resistivity and seismic refraction survey across the SE margin of Lake Ngami, NW Botswana. Acta Geophysica. 5(3):28–42.

Slater, LD, Sandberg, SK. 2000. Resistivity and Induced Polarization Monitoring of Salt water Transport under Natural Hydraulic Gradients: Geophysics 65, 408–420.

Sojobi AO, Balogun II, Salami AW. 2016. Climate change in Lagos State, Nigeria: what really changed?. Environ Monit Assess. 188(10):556. doi:10.1007/s10661-016-5549-z

Soupios PM, Georgakopoulos P, Papadopoulos N, Saltas V, Andreadakis A, Vallianatos F, Sarris A, Makris JP. 2007. Use of engineering geophysics to investigate a site for a building foundation. J Geophys Eng. 4(1):94–103. doi:10.1088/1742-2132/4/1/011

Stiebel D. 2011. Protocol for free field measurement of mitigation effects. Noise and Vibration Mitigations for Rail Transportation Systems, D1.2: 1–25.

Taipodia J, Baglari D, Biswas S, Dey A 2015. Dispersion analysis using active masw survey data. 50th indian geotechnical conference 17th – 19th December 2015, Pune, Maharashtra, India.

Tokimatsu K, Tamura S, Suzuki H, Katsumata K. 2012. Building damage associated with geotechnical problems in the 2011 Tohoku Pacific Earthquake. Soils and Foundations. 52(5):956–974. doi:10.1016/j.sandf.2012.11.014

Uhlemann SS, Sorensen JPR, House AR, Wilkinson PB, Roberts C, Gooddy DC, Binley AM, Chambers JE. 2016. Integrated time-lapse geoelectrical imaging of wetland hydrological processes. Water Resour Res. 52 (3):1607–1625. doi:10.1002/2015WR017932

Usmen MA, Vilnitis M. 2015. Evaluation of safety, quality and productivity in construction IOP conf. series: materials science and engineering 96; 012061Vinh, P. C. & Malischewsky, P. G. (2007). an approach for obtaining approximate formulas for the rayleigh wave velocity. Wave Motion. 44:549–562.

Van Dam RL. 2012. Landform characterization using geophysics-recent advances, applications, and emerging tools. Geomorphology. 137(1):57–73. doi:10.1016/j.geomorph.2010.09.005

Xia J, Miller RD, Park CB, Hunter JA, Harris JB, Ivanov J. 2002. Comparing shear-wave velocity profiles inverted from multichannel surface wave with borehole measurements. Soil Dynamics and Earthquake Engineering. 22(3):181–190. doi:10.1016/S0267-7261(02)00008-8

Yan H, Ming-Xiang Z. 2001. Study on Wetland Loss and Its Reasons in China: Chinese Geographical Science Journal. 11:245–252.